PAM-NL: A GENERAL FINITE ELEMENT PROGRAM FOR THE NONLINEAR THERMOMECHANICAL ANALYSIS OF STRUCTURES

E. HAUG, J. M. LOCCI
Engineering System International S.A.,
20 rue Saarinen, F-94150 Rungis Silic, France

F. C. ARNAUDEAU
Novatome Industries, 20 Avenue Edouard Herriot, F-92350 Le Plessis Robinson, France

Summary

This paper presents the concepts, features, organization, application problems and qualification tests of the general purpose finite element analysis program PAM-NL. The features include thermomechanical analysis, eigenvalue buckling, plasticity, creep, dynamic direct integration, nodal constraint options and functional load description.

The incremental equations of motion are based on the total Lagrange formulation.

The basic solution scheme is implicit incremental with equilibrium correction after each load or time increment. A full and modified Newton-Raphson iteration scheme is also available and it may be used e.g. in large displacement elastic analyses. The code uses the efficient skyline out of core equation solving technique.

Three types of Lagrange constraints between nodal degrees of freedom permit master-slave node analysis, convenient mesh grading, structural repetitivity, point symmetry and other more general constraints to be simulated conveniently.

The code contains isoparametric thick shell, three dimensional and two dimensional solid elements. A thin shell and a beam element using numerical integration across the thickness and a contact spring element are included. The elements can have large Green Strains, thermo-elasto-plasticity and creep. Some elements can remain linear throughout the analysis. Orthotropic elastic and plastic features allow the analysis of fiber reinforced composite structures.

For metals isotropic and kinematic hardening plasticity models and creep models, all with temperature dependent material constants, are available, together with specialized models for cyclic behavior.

For concrete, soils, rocks, specialized constitutive models, with moduli being functions of confining stress, and with peak and residual strength parameters to model post rupture, are available with the anisotropic solid elements.

A version of the code,called NOV-NL, including special capabilities (e.g.:axisymmetric thin shell elements) has been implemented and extended at Novatome, for the analysis of LMFBR components.

The use of PAM-NL and its post processors as a practical nonlinear analysis tool are demonstrated on selected example problems in nuclear technology and other fields : elasto plastic collapse analysis, weld residual stress analysis, thermoplastic cyclic analysis, nonlinear dynamic pressure impulse, buckling eigen-value extraction, and others.

1. Basic Features of PAM-NL

The code PAM-NL is a general implicit three-dimensional nonlinear finite element program, with large displacements and large deformations, for the thermo-elasto-plastic and creep analysis of structural systems subjected to static and dynamic loads.

The method of analysis utilizes an incremental-iterative finite element procedure, based on a rigorous and complete nonlinear formulation. In dynamic analyses the generalyzed Newmark-Wilson $\beta - \gamma - \theta$ implicit operator is used for the direct integration of the discretized equations of motion. A built-in eigenvalue search module allows the evaluation of static buckling modes and eigenvalues and dynamic modes and frequencies at any stage of an analysis. Lagrange multiplier options can be used for constraining nodes and the program has complete restart capabilities.

The finite element standard library comprises the following elements : a 16 node isoparametric element (48 degrees of freedom) for thick shells and solids, an 8 node isoparametric brick element (24 degrees of freedom) for 3D solids, a 4 node quadrilateral isoparametric element (8 degrees of freedom) for axisymmetric solids and 2D and 3D membranes, a thin plate and shell element (24 degrees of freedom after Felippa and Sharifi /2/), a prismatic 3D beam element, with possibility of excentricity (e.g. for modelling excentric stiffeners), and a contact spring element for modelling variable contact between structures and supports.

The modular built-up of the code permits easy branching of new element types. Variable node isoparametric 2D and 3D elements and a multilayered composite thin shell will be branched in the near future.

The standard material constitutive models of the code, being implemented for each element type, are described in chapter 2. The code is modular in the sense that to each element type a new material type can be branched easily. This is especially important in view of the rapidly developing material laws in todays industrial applications. The following non-standard material types have been branched to some of the element types : anisotropic plasticity (e.g. composite materials), multi-criteria plastic models with coupled damage modes (Dubois /5/), ubiquitous joint rock plastic model, concrete coupled damage mode models, primary creep models, etc...

The following static and dynamic load types are available : imposed displacements and variable boundary conditions, concentrated loads, uniform temperature and gradients, conservative and non-conservative normal and tangent pressures, acceleration type body force loads in all directions, and centrifugal forces with and without the effects of radial displacements. All loads are described via functions in time, which may be shifted for convenient description of transient effects, and which are activated via specified function numbers at nodes and elements. Nodal masses, velocities and dashpots and element masses complete the description of the system to be analyzed in dynamic analyses.

2. Theoretical outline

The total Lagrange implicit incremental/iterative finite element discretization procedure used in the code has been described many times in the literature, e.g. see Sharifi/1/, and only a brief account of the basic theoretical features is given.

2.1. Kinematics. In a total Lagrange approach, Green strains may be used as an objective measure of deformation, and they follow from, i,j = 1, 2, 3

$$E_{ij} = \varepsilon_{ij} + \bar{\varepsilon}_{ij} + \eta_{ij} \qquad (1)$$

in which E_{ij} = Green strain increment tensor components, $2\varepsilon_{ij} = u_{i,j} + u_{j,i}$ = linear strain increment, $2\bar{\varepsilon}_{ij} = {}^1u_{k,i}\, u_{k,j} + u_{k,i}\, {}^1u_{k,j}$ = linear strain increment depending on initial displacements, $2\eta_{ij} = u_{k,i}\, u_{k,j}$ = nonlinear strain increment, u_i = global displacement increments, and ${}^1u_i$ = global total displacements in a deformed configuration, 1. An input parameter allows the analysis to be performed for arbitrarily large strains, eq.(1), or using the linear strain parts only, through which nonlinear and initial displacement effects may be switched off optionally.

2.2. Incremental Equations of Motion and Solution. The total Lagrange formulation leads to the incremental global matrix equations of motion

$$ {}^1M\, \ddot{u} + {}^1C\, \dot{u} + {}^1K_T\, u = {}^2\hat{R} \qquad (2)$$

in which ${}^2\hat{R} = {}^2R - {}^1F^R - {}^1F^I - {}^1F^C$ corresponds to the dynamic load vector, ${}^1M$, ${}^1C$, ${}^1K_T$ are the global mass, damping and tangent stiffness matrices, respectively, and ${}^1F^R$ = structure internal resisting forces, ${}^2R$ = externally applied loads at time $t + \Delta t$, ${}^1F^I = {}^1M\, {}^1\ddot{u}$ = structural inertia forces, and ${}^1F^C = {}^1C\, {}^1\dot{u}$ = structural damping forces. This equation can be solved iteratively within each time or load step with an update of all forces and with or without an update of the tangent stiffness matrix with subsequent factorization. The code allows also for a sporadic reformation of the stiffness matrix, where this matrix is kept constant over a user-specified number of time or loads steps. Moreover, some element groups can remain linear for all or some of the analysis increments, thus saving additional computer time for element stiffness formation.

The β- γ-θ discretization scheme implemented in the code relates displacement increments, velocities and accelerations as follows, using $\Delta u = {}^2u - {}^1u$,

$$\begin{aligned} {}^2\ddot{u} &= a_o\, \Delta u - a_1\, {}^1\dot{u} - a_2\, {}^1\ddot{u} \\ {}^2\dot{u} &= b_o\, \Delta u - b_1\, {}^1\dot{u} - b_2\, {}^1\ddot{u} \end{aligned} \qquad (3)$$

where left hand superscript, 2, corresponds to time $t + \Delta t$, and where the coefficients are

a_o	a_1	a_2	b_o	b_1	b_2
$\frac{1}{\beta(\theta\Delta t)^2}$	$\frac{1}{\beta(\theta\Delta t)}$	$\frac{1}{2\beta} - 1$	$\frac{\gamma}{\beta(\theta\Delta t)}$	$\frac{\gamma}{\beta} - 1$	$(\frac{\gamma}{2\beta} - 1)\ (\theta\Delta t)$

For $\theta = 1$, $\gamma = 1/2$, $\beta = 1/4$, one obtains the trapezoidal rule (Newmark constant average acceleration scheme), for $\theta \geq 1.37$, $\gamma = 1/2$, $\beta = 1/6$, one obtains the Wilson operator, for $\theta = 1$, $\gamma > 1/2$ and $\beta \geq 1/4\ (\gamma + 1/2)^2$ one obtains an unconditionally stable Newmark scheme, which introduces an often desired numerical dissipation.

2.3. Standard Nonlinear Constitutive Models. The incremental strain tensor is supposed to be small enough so it can be decomposed into the elastic (E), thermal (T), plastic (P) and creep (C) increments according to

$$E_{ij} = E^E_{ij} + E^T_{ij} + E^P_{ij} + E^C_{ij} \qquad (4)$$

The elastic component follows from the expression

$$E^E_{ij} = {}^1H_{ijkl} \left(s_{kl} - \frac{{}^2E - {}^1E}{{}^1E}\, {}^1s_{kl} \right) \qquad (5)$$

where ${}^1H_{ijkl}$ = usual isotropic elastic compliance tensor, s_{kl} = increments in 2-nd Piola-Kirchhoff stress tensor, being conjugate to the Green strain tensor, ${}^1s_{kl}$ = initial stresses, ${}^2E$, ${}^1E$ = Youngs moduli at time $t + \Delta t$, and t, respectively. The thermal component follows

from $E^{T}_{ij} = {}^{1}\alpha_{T} \; \theta \; \delta_{ij}$ (6)

with ${}^{1}\alpha_{T}$ = temperature dependent coefficient of thermal expansion, $\theta = {}^{2}\theta - {}^{1}\theta$ = temperature increment and δ_{ij} = Kronecker symbol.

The plastic von Mises strain component follows for normal plastic flow from the expressions $E^{Pi}_{ij} = \frac{{}^{1}E - {}^{1}E_{t}}{{}^{1}E \; {}^{1}E_{t}} \left(\frac{3}{2\,{}^{1}\bar{\sigma}}\right)^{2} {}^{1}t_{ij} \; {}^{1}t_{kl} \; s_{kl} + \frac{3}{2\,{}^{1}\bar{\sigma}} \; {}^{1}\phi \; \theta \; {}^{1}t_{ij}$ (7)

for isotropic hardening, and from

$$E^{Pk}_{ij} = \frac{{}^{1}E - {}^{1}E_{t}}{{}^{1}E \; {}^{1}E_{t}} \left(\frac{3}{2\bar{\sigma}_{o}}\right)^{2} ({}^{1}t_{ij} - {}^{1}\alpha_{ij}) ({}^{1}t_{kl} - {}^{1}\alpha_{kl}) s_{kl} + \frac{3}{2\bar{\sigma}_{o}} \; {}^{1}\phi\theta \, ({}^{1}t_{ij} - {}^{1}\alpha_{ij}) \quad (8)$$

for kinematic hardening. In above expressions, ${}^{1}E_{t}$ = plastic tangent modulus, ${}^{1}\bar{\sigma} = \sqrt{3/2 \; {}^{1}t_{ij} \; {}^{1}t_{ij}}$ = equivalent stress, ${}^{1}t_{ij} = {}^{1}s_{ij} - 1/3 \; \delta_{ij} \; {}^{1}s_{kk}$ = deviatoric stress, ${}^{1}\phi = \partial \, {}^{1}\bar{\varepsilon}^{P} / \partial \theta$ = increment in plastic strain due to temperature change at constant stress, ${}^{1}\alpha_{ij}$ = shift tensor, translating the von Mises yield surface in deviatoric stress space, and $\bar{\sigma}_{o}$ = initial effective yield stress. Material properties can vary with temperature.

The Norton-Odqvist steady state creep strain increment is given by

$$\begin{aligned} E^{C}_{ij} &= 3/2 \; \Delta t \; {}^{1}\bar{\sigma}^{(n-1)} \, ({}^{1}\beta + 1/2\beta) \; {}^{1}t_{ij} \\ &+ 3/4 \; \Delta t \; {}^{1}\bar{\sigma}^{(n-1)} \, ({}^{1}\beta + 2/3\beta) \; L_{ijkl} \; s_{kl} \\ &+ 9/8 \; \Delta t \; {}^{1}\bar{\sigma}^{(n-3)} \, ({}^{1}\beta + 2/3\beta) \; {}^{1}t_{ij} \; {}^{1}t_{kl} \; s_{kl} \end{aligned} \quad (9)$$

where $\dot{E}^{C}_{ij} = 3/2 \; {}^{1}\beta \; {}^{1}\bar{\sigma}^{(n-1)} \; {}^{1}t_{ij}$ = basic creep rate formula, ${}^{1}\beta$, n = material constants, $\beta = {}^{2}\beta - {}^{1}\beta$ = change in β due to a change in temperature, $L_{ijkl} = 1/2 \, (\delta_{ik} \, \delta_{jl} + \delta_{il} \, \delta_{jk}) - 1/3 \delta_{ij} \, \delta_{kl}$ and Δt = selected creep time increment.

Substitution of eqs. (5) - (9) into eq. (4) leads to the incremental strain-stress law, which can be inverted to give the incremental stress-strain law used in the finite element formulation.

2.4. Eigenvalue Extraction. Buckling eigenvalue extraction is based on the following characteristic equation

$$\det \left[{}^{p}K_{T} \, ({}^{p}u, \, {}^{p-1}\sigma) + \lambda \, ({}^{p+1}K_{T} \, ({}^{p+1}u, \, {}^{p}\sigma) - {}^{p}K_{T} \, ({}^{p}u, \, {}^{p-1}\sigma)) \right] \quad (10)$$

in which, for $p \geq 1$, ${}^{p}K_{T} = {}^{p}K_{EP} \, ({}^{p}u) + {}^{p}K_{G} \, ({}^{p-1}\sigma)$ = tangent stiffness matrix in configuration, p, depending on the displacements, ${}^{p}u$, of this configuration and on the stresses, ${}^{p-1}\sigma$, of the previous position, p-1, and where K_{EP}, K_{G} are the elasto-plastic and the "geometric" stiffness, respectively. The first buckling force vector follows from

$${}^{p}R_{c1} = {}^{p-1}R + \lambda_{1} \, ({}^{p}R - {}^{p-1}R) \quad (11)$$

in which ${}^{p-1}R$ = mode of loading leading to configuration p-1, ${}^{p}R = {}^{p-1}R + \Delta R$ = mode of loading leading to configuration p. Above equations can be interpreted as to find the buckling eigenvalues of the structure, preloaded by forces ${}^{p-1}R$, due to an additional loading, ΔR.

2.5. Lagrange Constraints. The built-in Lagrange constraint option minimizes the value

$$1/2 \; u^{T} K u - u^{T} R \quad (12)$$

subject to the set of M linear constraint equations, i = 1,...,M

$$\sum_{j=1}^{N} \alpha_{ij} \, u_{j} = 0 \quad (13)$$

The user can specify three different types of constraints, namely the usual multi-point rigid master-slave condition, a multi-point flexible constraint condition, e.g. for enfor-

cing inter-element compatibility for discontinuous mesh grading, in which a number of slave nodes are attached to two masters via flexible beam shape functions of an imaginary beam between the two master nodes, which flexes according to their displacements and rotations, and a possibility to define directly arbitrary constraints of the type given by eq. (13).

3. Applications.

Out of many benchmark tests and industrial applications of the code, a few examples with bearing on nuclear safety analysis are presented.

3.1. Tension-Torsion Problem /3/. A state of uniaxial tension and shear, as it arises when a thin walled tube is subject to an axial tensile force and to a torsion moment, is applied to a two-dimensional 4 node element in a combination shown in Fig.1a, with material properties according to the stress strain diagram of Fig. 1b. The resulting elasto-plastic axial and shear stresses are shown in Fig. 1c and 1d, and the corresponding calculated axial and shear strains differ maximally by 2 % from the average calculated values of reference/3/.

3.2. Plate with Circular Hole /3/. One quarter of a rectangular plate with dimensions 17.74 x 35.46 x 1.27 cm with a central hole of 3.18 cm in diameter, has been modelled as shown in Fig. 2a, according to the ANSYS/ADINA grid described in reference/3/, using isoparametric 4 node element with only 4 integration points vs. 9 points of the reference. The plate is pulled longitudinally with a force reaching 1600 daN. The bilinear material has an elastic modulus of 15.0 MPa, a tangent modulus of 0.426 MPa, Poissons ratio = 0.3, and a yield stress of 60.5 MPa. The average stress due to 1600 daN lies with 71 MPa above the yield stress, so that at the final force level all points of the plate have yielded.

Fig.2b shows the lines of equal axial strain, which compare very favorably with the results of the reference, which seem to be based on a more refined integration while using the same finite element grid.

3.3. Pinched Cylinder. An infinitely long cylinder with a circumferential line load applied inward in radial direction as shown in Fig. 3a, has been modelled using 220 thin shell elements. The load has been introduced via non-conservative pressures on one ring of elements. Theory predicts an axially damped out radial buckling wave pattern of 22 full sinusoidal waves near the loaded circumference, see Fig. 3b, meaning that one full sinusoidal wave will be represented by just four thin shell elements. Despite this rather crude mesh, both, the buckling eigenvalue prediction (λ = 0.9987) and the incremental collapse analysis (onset at λ = 0.98), compare very favorably with the predicted theoretical value of λ=1.000, as shown in Fig. 3c.

3.4. Elastic Dynamic Snap Buckling /4/. The Newmark constant average acceleration scheme has been used to verify the critical step normal pressure, P_{crit}, of a shallow, hinged, circular arch, modelled by 10 beam elements using symmetry, as shown in Fig. 4a. For an opening of 2 times 15°, radius R = 67.115 in (170.47 cm), thickness h = 1.0 in (2.54 cm), elastic modulus E = 10 x 10^6 lb/in^2 (0.704 daN/cm2), Poissons ratio = 0.2 and mass density δ = 2.44 x 10^{-4} lb sec^2/in^4 (5.86 x 10^6 daN sec^2/cm^4), Fig. 4b indicates that the critical step pressure for snap through lies between 444.0 and 450.0 lb/in^2 (31.24 and 31.67 daN/cm^2), which agrees very closely with the results found by Bathe /4/.

3.5. Numerical Weld Simulation /6/. An axisymmetric simulation of an electron beam welding process, connecting two hemispherical thick walled metal shells, has been simulated via an axisymmetric 4 node finite element layout, shown in Fig.5a, using somewhat idealized temperature dependent material properties, shown in Fig. 5b. The initial temperature field

with a liquid zone of molten metal and very high temperature gradients is seen in Fig. 5c.

Departing from this state, the analysis procedes in ca.100 analysis increments, during which the first rapidly spreading and then slowly cooling transient temparature field, obtained by a heat transfer code, is applied in each step to the material with highly temperature dependent properties, up to the time when thermal equilibrium in the shell has been reached. Fig. 5d shows a succession of intermittent stages and Fig. 5e presents the final residual state of deformation and von Mises equivalent stress, using isotropic hardening.

The reported good agreement of numerical and experimental residual deformations show that the code enables the study of a complex thermo-mechanical phenomenon by relatively simple means.

3.6. Crushing Strength of Helicopter Components. In a numerical elasto-plastic incremental collapse analysis, which accompanied an experimental test program, the aluminum stiffened panel side walls of the fuel compartments of a helicopter have been subjected to in-panel imposed displacements, applied at the rounded panel ends in the direction of the stiffeners, as shown in Fig. 6a. Using structural repetitivity and ca. 160 thin shell and excentric beam and contact elements, Figs.6b show the deformed states of the analyzed portion within a total of 24 static load increments.

The resisting force vs. displacement curve is compared in Fig. 6c with the experimental values, showing excellent agreement in intermittent and final average peak force. Due to e.g. lack in predeformations, however, the numerical model seems initially to be much stiffer than the tested structure. The corresponding energy absorption curve of Fig. 6d shows also good agreement with the experiments.

References

(1) SHARIFI P., and YATES D.N., "Nonlinear Thermo-Elasto-Plastic and Creep analysis by the Finite Element Method", AIAA Journal, Vol. 12, Sept. 1974, pp 1210-1215.

(2) SHARIFI P., "Nonlinear Buckling Analysis of Composite Shells", AIAA Journal, Vol.13, n° 6, June 1975, pp 726-734.

(3) CLINARD J.A., et al., "Verification by Comparison of Independent Computer Program Solutions", Pressure Vessels and Piping Computer Program Evaluation and Qualification, PVP - PB - 024 - ASME 1977.

(4) BATHE K.J., et al., "Finite Element Formulations for Large Displacement and Large Strain Analysis", Report N° UC-SESM 73-14, University of California, Berkeley.

(5) DUBOIS J., "Coupled Damage Modes (CDM) Plasticity Models for the Simulation of Complex Materials used in Reactors", SMIRT V, paper in section M, 1979.

(6) LOCCI J.M., et al., "Finite Element Simulation of the Welding Process and Structural Behavior of Welded Components", SMIRT IV, paper L 4/5, 1977.

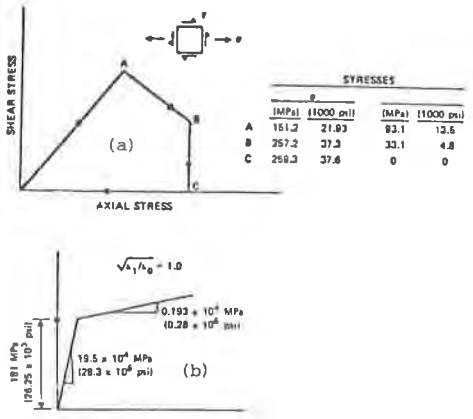

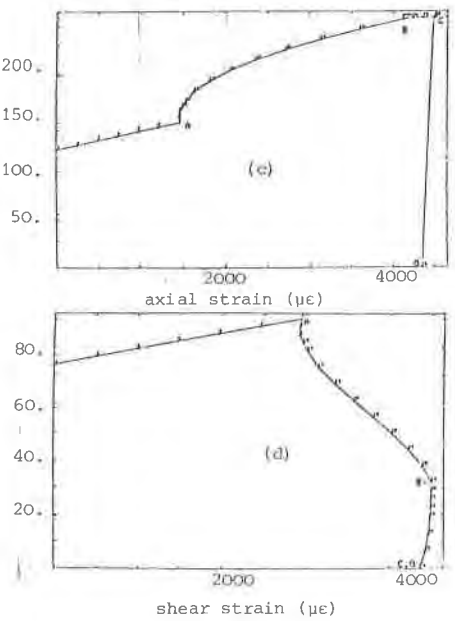

Fig. 1 : Tension-Torsion Problem /3/

(a) applied shear and axial stress

(b) material stress-strain diagram

(c) axial stress vs. axial deformation

(d) shear stress vs. shear deformation

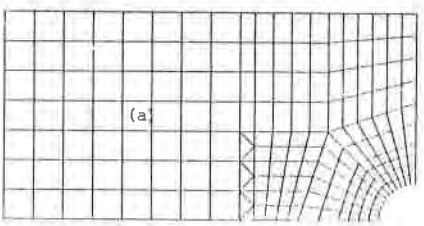

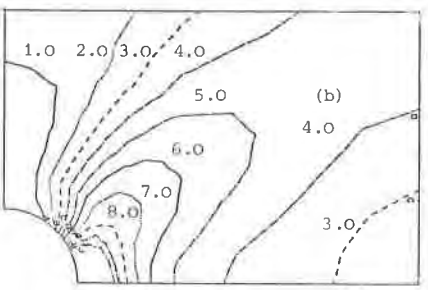

Fig. 2 : Plate with Circular Hole /3/

(a) finite element mesh

(b) lines of equal axial strain ($* 10^{-2}$)

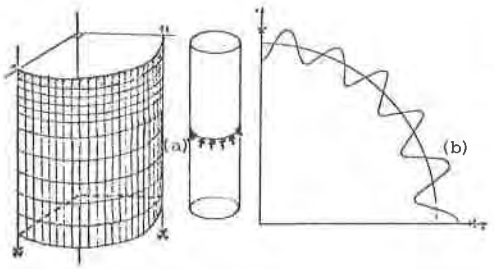

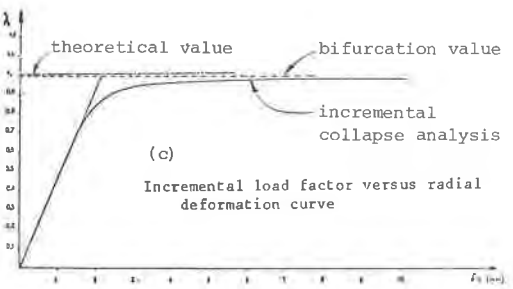

Fig. 3 : Pinched Cylinder

(a) finite element mesh

(b) buckling wave pattern near the load (c) predicted eigenvalue

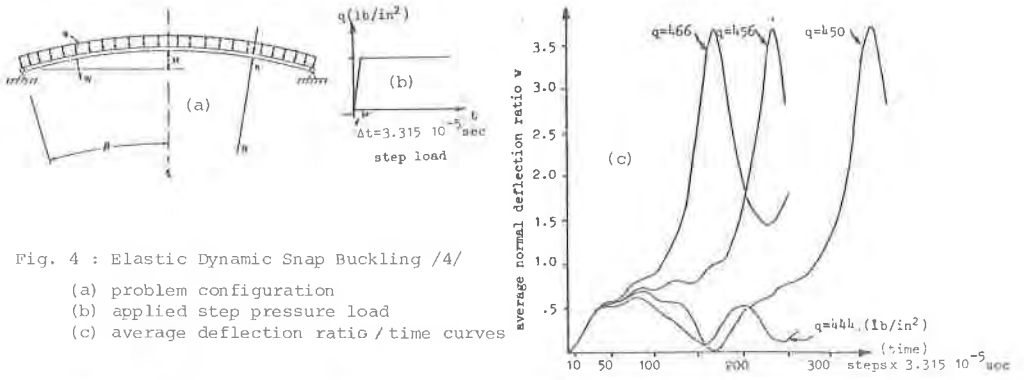

Fig. 4 : Elastic Dynamic Snap Buckling /4/

(a) problem configuration
(b) applied step pressure load
(c) average deflection ratio / time curves

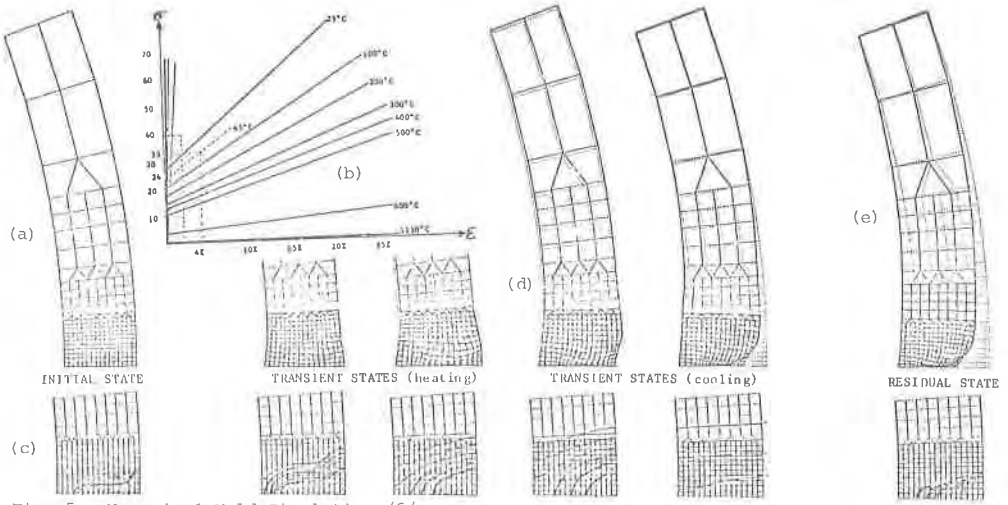

Fig. 5 : Numerical Weld Simulation /6/

(a) finite element mesh, (b) thermomechanical properties
(b) initial heat input, (d) intermittent stages
(c) final state

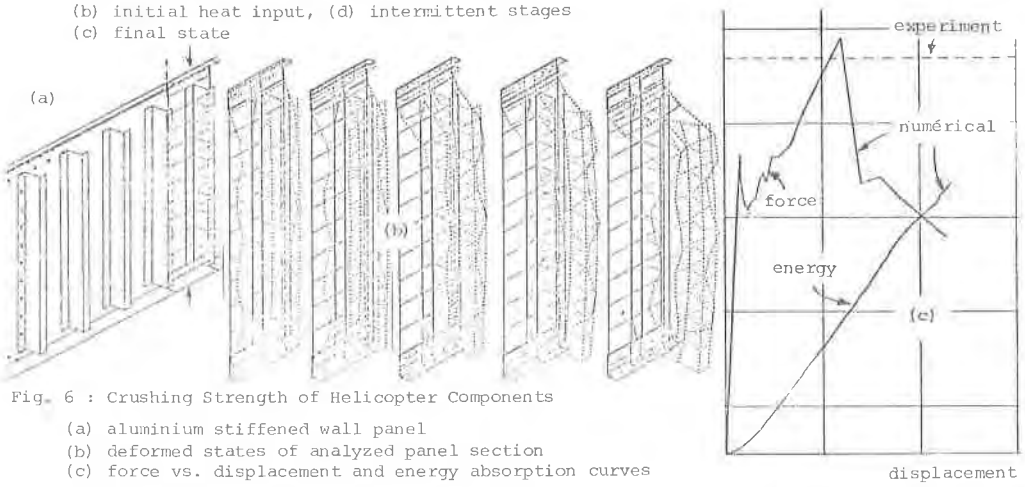

Fig. 6 : Crushing Strength of Helicopter Components

(a) aluminium stiffened wall panel
(b) deformed states of analyzed panel section
(c) force vs. displacement and energy absorption curves